Special Collection

Large-Scale Synthesis of Nanostructured Carbon-Ti$_4$O$_7$ Hollow Particles as Efficient Sulfur Host Materials for Multilayer Lithium-Sulfur Pouch Cells

Shilin Mei,[a] Andreas Siebert,[b] Yaolin Xu,[a] Ting Quan,[a] Raul Garcia-Diez,[b] Marcus Bär,[b, c, d, e] Paul Härtel,[f] Thomas Abendroth,[f] Susanne Dörfler,[f] Stefan Kaskel,[f] and Yan Lu*[a, g]

Applications of advanced cathode materials with well-designed chemical components and/or optimized nanostructures promoting the sulfur redox kinetics and suppressing the shuttle effect of polysulfides are highly valued. However, in the case of actual lithium-sulfur (Li–S) batteries under practical working conditions, one long-term obstacle still exists, which is mainly due to the difficulties in massive synthesis of such nanomaterials with low cost and ease of control on the nanostructure. Herein, we develop a facile synthesis of carbon coated Ti$_4$O$_7$ hollow nanoparticles (C–Ti$_4$O$_7$) using spherical polymer electrolyte brush as soft template, which is scalable via utilizing a minipilot reactor. The C–Ti$_4$O$_7$ hollow nanoparticles provide strong chemical adsorption to polysulfides through the large polar surface and additional physical confinement by rich micro- & mesopores and have successfully been employed as an efficient sulfur host for multilayer pouch cells. Besides, the sluggish kinetics of the sulfur and lithium sulfide redox mechanism can be improved by the highly conductive Ti$_4$O$_7$ via catalyzation of the conversion of polysulfides. Consequently, the C–Ti$_4$O$_7$ based pouch cell endows a high discharge capacity of 1003 mAh g^{-1} at 0.05 C, a high-capacity retention of 83.7% after 100 cycles at 0.1 C, and a high Coulombic efficiency of 97.5% at the 100th cycle. This work proposes an effective approach to transfer the synthesis of hollow Ti$_4$O$_7$ nanoparticles from lab- to large-scale production, paving the way to explore a wide range of advanced nanomaterials for multilayer Li–S pouch cells.

[a] Dr. S. Mei, Dr. Y. Xu, Dr. T. Quan, Prof. Dr. Y. Lu
Department for Electrochemical Energy Storage
Helmholtz-Zentrum Berlin für Materialien und Energie GmbH
Hahn-Meitner Platz 1, 14109 Berlin, Germany
E-mail: yan.lu@helmholtz-berlin.de
[b] Dr. A. Siebert, Dr. R. Garcia-Diez, Prof. Dr. M. Bär
Department Interface Design
Helmholtz-Zentrum Berlin für Materialien und Energie GmbH
Albert-Einstein-Str. 15, 12489 Berlin, Germany
[c] Prof. Dr. M. Bär
Energy Materials In-Situ Laboratory Berlin (EMIL)
Helmholtz-Zentrum Berlin für Materialien und Energie GmbH
Albert-Einstein-Str. 15, 12489 Berlin, Germany
[d] Prof. Dr. M. Bär
Helmholtz-Institute Erlangen-Nürnberg for Renewable Energy (HI ERN)
Albert-Einstein-Str. 15, 12489 Berlin, Germany
[e] Prof. Dr. M. Bär
Department of Chemistry and Pharmacy
Friedrich-Alexander-Universität Erlangen-Nürnberg (FAU)
Egerlandstr. 3, 91058 Erlangen, Germany
[f] P. Härtel, Dr. T. Abendroth, Dr. S. Dörfler, Prof. Dr. S. Kaskel
Fraunhofer Institute for Material and Beam Technology (IWS)
Winterbergstr. 28, 01277 Dresden, Germany
[g] Prof. Dr. Y. Lu
Institute of Chemistry
University of Potsdam
14467 Potsdam, Germany

Introduction

Lithium-sulfur (Li–S) cells have received tremendous recognition in recent years both from a scientific and industrial perspective due to the high theoretical capacity (∼1675 mAh g^{-1}), as well as the cheap and environmentally friendly characteristics of sulfur used as active materials in the cathode.[1] Nevertheless, the practical application has been greatly impeded due to some notorious problems of lithium anode and sulfur cathode. The so-called "shuttle effect" of lithium polysulfides in state-of-the-art ether-based (dimethoxyethane/dioxolane, DME/DOL) electrolytes during cycling process,[1b,d] the insulating nature of sulfur and its full discharge products (Li$_2$S, Li$_2$S$_2$), together with the large volume expansion resulting from the insertion of Li$^+$, will lead to a quick decrease of the electrochemical utilization for both coin cells and pouch cell batteries. In order to tackle these issues, research efforts have been intensified to develop cathode materials having unique chemical properties with porous structure to confine the polysulfide intermediates and to maintain the high electronic conductivity to improve the sluggish redox kinetics.[1e,2] Various functional materials (e.g., carbonaceous materials, metal oxides and sulfides, and polymers) have demonstrated capability of diminishing the dissolution of polysulfides in the electrolyte through physical- and chemical-confinement strategies.[2b,e]

However, most of the cathode designs involve complicated synthetic techniques to build up attracting chemical and

Batteries & Supercaps

Research Article
doi.org/10.1002/batt.202100398

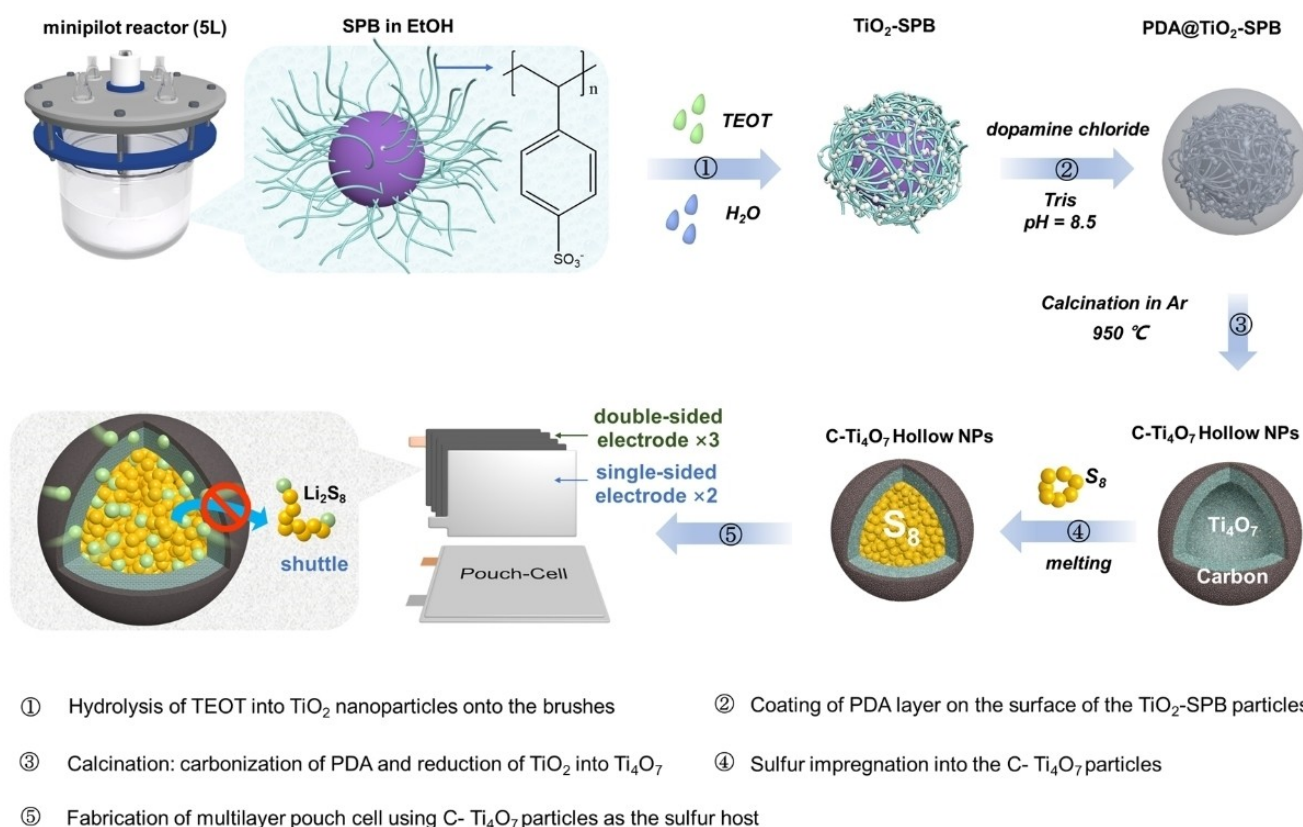**Chemistry Europe**
European Chemical
Societies Publishing

physical structures that can ultimately solve the aforementioned problems, leading to high cost and low production yield of the "lab-born" materials. Moreover, although highly efficient cathode materials with valuable functions are frequently reported, there is still a large gap between lab cell construction and prototype cell development. Besides, outstanding performances can only be achieved in coin cells at the cost of uneconomical consumables such as excess lithium and electrolyte. In contrast, multilayer pouch cells have rarely achieved performances as excellent as that of coin cells so far due to the difficulties in massive synthesis of advanced cathode materials and low cycle stability when practically relevant electrolyte amounts (< 5 μL mg^{-1} sulfur) and lithium foils (< 100 μm) are employed.[3] Therefore, rapid transfer of material synthetic technologies from lab cell to the prototype cell level is essential as well for the commercialization of Li–S batteries. Fundamental studies on large-scale synthesis of efficient cathode materials, e.g., those combining both the active components with well-designed nanostructures that are usually easy to be achieved in lab level, should be paid with increasing attention to break one of the bottlenecks toward the commercialization of Li–S cells.[3d,e,4]

Based on the tremendous efforts and promising results in coin cells,[2c,e,5] the design of cathode materials for pouch cells is of high interest, and it is important to establish strategies to produce these materials at low cost by maintaining their high performance. Among the current explored sulfur/polysulfide-fixing strategies, creating both chemical adsorption and physical confinement for polysulfides has been demonstrated to be highly efficient. In such design, polar surface provided by metal oxides/sulfides can strongly adsorb soluble polysulfides for minimizing the diffusion of polysulfide into the cell and enhancing the reaction kinetics of the overall cell reaction. Besides, hierarchical porous structure and good conductivity are also preferred to facilitate electrolyte infiltration and to promote fast Li-ion diffusion and electron transfer. Therefore, the synthesis of conductive metal oxides/sulfides with porous structures has been extensively reported and brought ongoing improvement to coin cell performances.

Except for the valuable functions of normal metal oxides/sulfides, creating "atomic defects" has been popular to induce better conductivity and catalytic sites to sulfur redox. Recently, both theoretical and experimental research has demonstrated the Magnéli phase Ti$_4$O$_7$ to be an outstanding candidate as efficient Li–S cathodes or interlayer materials, which can significantly hinder the polysulfide shuttle effect and regulate the Li$_2$S deposition.[6] As a representative of titanium suboxide (Ti$_n$O$_{2n-1}$), Ti$_4$O$_7$ shows a high conductivity (1.0×10^5 S m^{-1}) that is eleven magnitude higher than that of TiO$_2$ ($< 10^{-6}$ S m^{-1}).[6h,7] Moreover, the structure of Ti$_4$O$_7$ is based on rutile TiO$_2$ crystal lattice and is chemically stable, which can be generated from partial reduction of TiO$_2$, thus it has abundant sources in nature. Specifically, Ti$_4$O$_7$ contains polar O–Ti–O units and large charge densities at the defects that have a high affinity for polysulfide, which can enhance the interaction with the polysulfide intermediates, lowering the thermodynamic barriers and promoting the kinetics of the polysulfide conversion.[6d,7a,8]

In addition to chemical adsorption of soluble polysufides on the polar surface of Ti$_4$O$_7$, an optimized porous structure is essential to improve the utilization of the active sulfur and Li$_2$S. On the one hand, the porous structure is important to induce a facile uptake of sulfur species and electrolyte, which can realize a practical relevant sulfur loading, fast diffusion of electrolyte, and uniform redox reactions. On the other hand, porous structure can provide additional physical confinement for polysulfides, which is beneficial for high-capacity retention upon long-term cycling.[9] However, producing porous Ti$_4$O$_7$ is challenging since it has been mainly synthesized by thermal reduction of TiO$_2$ at ca. 1000 °C with inert gas and carbon.[10] This method usually exposes its lost control on the uniform porous structures due to the growth of big crystals during the calcination. Recent advances have shown that templating methods work effectively in construction of porous Ti$_4$O$_7$.[6f,g] For instance, Caruso's group reported the synthesis of porous Ti$_4$O$_7$ particles with a surface area of 197.2 m^2 g^{-1} by using resol as pore-creating precursor.[11] Our group has improved the porous structure of Ti$_4$O$_7$ to a higher level by using a block copolymer, polystyrene-b-poly(2-vinylpyridine) (PS-b-P2VP), as soft template. A well-defined porous structure containing interconnected channels inside the particle has been produced, providing an extremely high surface area of 592.1 m^2 g^{-1}.[12] However, the above-mentioned templating methods still show their limitation for large-scale synthesis due to their complicated synthetic procedures and high cost of the sacrificial templates. Thus, developing a large-scale available synthesis approach with low cost and easy control on the porous structure has been a challenging and indispensable proposition so far.

Herein, a well-developed polymer template which is available for mass production, namely spherical polyelectrolyte brushes (SPB), has been proposed and successfully applied as an alternative template for the creation of porous Ti$_4$O$_7$ particles (Scheme 1). The template particles consist of a polystyrene core, from which long chains of poly(styrene sodium sulfonate) with rich negative charges are grafted. A novel photoreactor based on the flow-through UV module enables large-scale synthesis of such colloidal nanoparticles, which paves the way towards industrial applications.[13] Tetraethylorthotitanate [TEOT, Ti(OCH(CH$_3$)$_2$)$_4$] was applied as the precursor of Ti$_4$O$_7$, which is easily adsorbed onto the polymer brushes due to the strong coordination with the polymer brushes. The TEOT precursor firstly hydrolyzed in the presence of SPB, leading to the formation of well-dispersed TiO$_2$ nanoparticles. In order to improve the conductivity of the material as well as sustain the hollow and porous structure of Ti$_4$O$_7$, the TiO$_2$-SPB particles were coated with a thin layer of polydopamine (PDA), which can be converted to carbon after calcination in Argon. The calcination at 950 °C was necessary to induce the carbonization and partial reduction of TiO$_2$ to Ti$_4$O$_7$. Notably, the scale-up of synthesis can be easily realized by using a minipilot reactor up to 5 L, and 10 g of the products could be obtained from one batch after calcination. This quantity of hollow porous carbon-coated Ti$_4$O$_7$ nanoparticles (C–Ti$_4$O$_7$ NPs) with polar surface is sufficient for multilayer Li–S

Scheme 1. Scalable synthetic route of the carbon-coated Ti_4O_7 hollow particles using SPB as template and their application as cathode materials for multilayer Li–S pouch cells.

pouch cells. Besides, this strategy can be extended to a wide range of nanostructured metal oxides/sulfides, which show great potential as redox-mediators or polysulfide anchoring seeds in Li–S prototype cells.

Results and Discussion

Synthesis of carbon-coated Ti_4O_7 nanoparticles

SPB with rich negative charges can be applied as efficient template for the synthesis of organic/inorganic hybrid particles due to the counter ion exchange of the SPB particles with the inorganic precursors, which are usually positively charged. Besides, the charges of the brushes can be tuned according to the charge properties of inorganic precursors. Thus, the SPB particles with controllable charges represent an excellent soft template for the synthesis of complex nanostructures. In this work, SPB with negative charges provided by the long chains of poly(styrene sodium sulfonate) has been applied as template and TEOT was used as inorganic precursor. SPB templates with uniform shape and size (the average core diameter $d_{PS} \sim 80$ nm) are shown in Figure S1. The synthesis has been performed using a minipilot reactor as shown in Figure 1a. The TEOT can be hydrolyzed into TiO_2 through addition of trace amount of water. Figure 1b presents the spherical morphology of the TiO_2-SPB composite particles. We find that a layer of small inorganic

particles has been deposited onto the template surface (dark contrast), indicating the formation of TiO_2 from the hydrolysis of TEOT. It is well known that TEOT particles tend to be quickly hydrolyzed into TiO_2 and aggregated into big particles. In this work, the TiO_2 particles are homogeneously coated on the surface of PS cores – even at a higher scale of 10 g particles owing to the stabilization of the rich negative charges on the brushes, which results in the uniform nucleation followed by *in situ* growth of small TiO_2 particles (Figure 1b).

A polydopamine (PDA) layer has been coated on the surface of the TiO_2-SPB particles in order to stabilize the TiO_2 particles and sustain the spherical structure in the following calcination process (Figure S2). The calcination/carbothermal reduction step at 950 °C is essential for the generation of hollow porous $C-Ti_4O_7$ particles, which can remove the SPB template, simultaneously convert the PDA into carbon, and partially reduce TiO_2 into Ti_4O_7. During this process, the SPB template is mostly burnt out, leaving hollow space inside the particles. A part of the polymer is carbonized as well and reduces TiO_2 into Ti_4O_7 under the argon atmosphere. Figure 1(c and d) shows the SEM and TEM images of the $C-Ti_4O_7$ particles obtained in this way. The hollow structure due to the removal of the PS template is clearly visible. This good preservation of the hollow structure is mainly due to the PDA-converted carbon layer on the surface of the particles, where TiO_2 particles are stabilized and anchored by the PDA component, which hinders the formation of large aggregates during the thermal
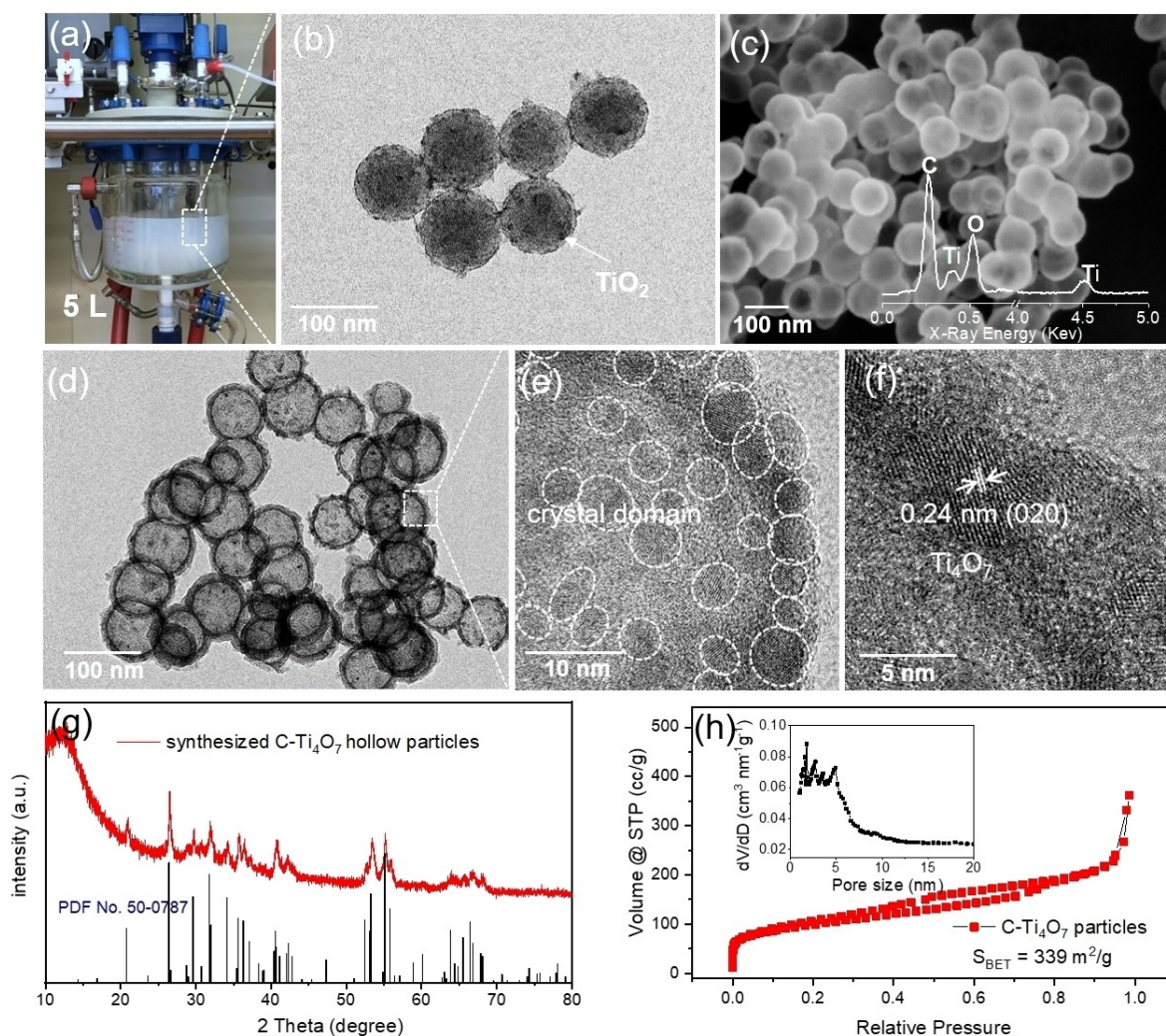
Figure 1. Synthesis and morphology characterization of the particles. a) Photo of the minipilot reactor. b) TEM image of the TiO_2-SPB composite particles. c) SEM and d) TEM images of the $C-Ti_4O_7$ hollow particles. Inset: EDS elemental spectra of the particles. e, f) High resolution transmission electron microscopy (HRTEM) images showing the crystalline structure of Ti_4O_7. g) XRD patterns of the $C-Ti_4O_7$ particles. h) Nitrogen adsorption/desorption isotherms of the $C-Ti_4O_7$ particles. Inset: Pore size distribution curve and the calculated specific surface area.

reduction process. In comparison, the particles without PDA coating are brittle after calcination and show collapsed structures and big aggregations, as shown in Figure S3.

In the synthesis of titanium oxides, the H_2O/Ti molar ratio, known as the hydrolysis ratio r, is a key factor in governing the size, morphology and crystallinity of the precipitates that form.[12] In this work, it is found that the hydrolysis ratio of 1:10 is appropriate to generate uniformly distributed small TiO_2 particles on the surface of SPB. Small size of TiO_2 is favorable for the transformation of TiO_2 to Ti_4O_7 via avoiding insufficient reduction of TiO_2 by carbon. In addition, a minimized particle size is also beneficial for utilization of the active surface of the host materials, thus can improve the specific energy density of the entire battery. A higher hydrolysis ratio results in big aggregations of TiO_2 particles (Figure S4). Thus, we choose $r = 1:10$ for the scalable synthesis of the $C-Ti_4O_7$ particles.

The crystal structure is characterized by HRTEM, and X-ray diffraction (XRD) as shown in Figure 1(e–g). HRTEM images

show the characteristic crystalline space of 0.24 nm corresponding to the (020) plane of Ti_4O_7. XRD patterns of the synthesized particles are compared with the standard Ti_4O_7 (ICDD card No. 500780, Figure 1g). The good agreement in the XRD patterns indicates that Ti_4O_7 is the primary crystalline phase of Magnéli. The specific surface area and porous structure of the particles have been further analyzed by N_2 adsorption/desorption measurement, which is displayed in Figure 1(h). The sharp increase of S_{BET} at low pressures ($P/P_0 < 0.05$) is due to the nitrogen filling in micropores below 2 nm, which is confirmed by the density functional theory pore size distribution curves (inset) derived from the N_2 adsorption branches. A distinct hysteresis loop can be observed with a typical type-IV isotherm, indicating the existence of a mesoporous structure. The pore size distribution curve shows both micropores and mesopores ranging from 0.9 to 4.9 nm. The Brunauer-Emmett-Teller (BET) specific surface area of the $C-Ti_4O_7$ particles is 339 $m^2 g^{-1}$ (Figure 1h), which contains the contribution of the outer

Batteries & Supercaps

Research Article
doi.org/10.1002/batt.202100398

Chemistry Europe
European Chemical
Societies Publishing

carbon layer. The mass ratio of Ti_4O_7 has been analyzed with TGA measurement, which is calculated to be 44.2 wt% in the composite based on the weight percentage of TiO_2 residual (Figure S5).

Chemical adsorption of lithium polysulfides to Ti_4O_7

Previous studies show that Magnéli phase Ti_nO_{2n-1} is a promising adsorber for polysulfides due to their polar O—Ti—O bonds while providing electric conductivity.[6d,11,12,14] The surface of Magnéli phase Ti_nO_{2n-1} has coordinatively unsaturated Ti centers due to regular oxygen vacancies arising from its unique crystal structure, therefore showing a high affinity to polysulfides. The capability of Ti_4O_7 to adsorb Li_2S_x is shown in Figure 2(a). Addition of C—Ti_4O_7 into the Li_2S_x solution results in a color change from light yellow to almost colorless upon mixing for 1 h, corresponding to a gradual decrease of the UV-vis absorption intensity in the range of 400–450 nm to almost zero (Figure 2b). Elemental mapping images of the collected precipitations show the homogeneous distribution of sulfur (Figure S6), which indicates the strong adsorption of Li_2S_x onto the C—Ti_4O_7 particles. After the visual test, the C—Ti_4O_7 particles were filtrated out of the solution and dried in an Ar-filled glovebox at 60 °C for 12 h. The Li_2S_x treated C—Ti_4O_7 particles (C—Ti_4O_7/Li_2S_x), C—Ti_4O_7 and the remainder of a dried Li_2S_x solution (Li_2S_x) were mounted with carbon tape on sample holders and measured with XPS, to further confirm the adsorption of Li and S on C—Ti_4O_7. The XPS survey spectra (shown in Figure S7) show the expected C, O, Ti, S, and Li peaks with additional Si and Ca contributions on the C—Ti_4O_7 sample originating from the carbon tape used to mount the powder samples. The S 2p Li_2S_x spectrum (see Figure S8) exhibits two major contributions with the S $2p_{3/2}$ contribution centered around 163.2 eV and 164.6 eV, while the S 2p spectrum of C—Ti_4O_7/Li_2S_x sample only shows one major peak with the S $2p_{3/2}$ contribution centered around 164.1 eV (together with signifi-

cant spectral intensity at higher binding energies, between 167 and 171 eV – most likely due to the presence/formation of sulfates, sulfites and/or thionates, thiosulfates). This is not only evidence for an adsorption of S on the C—Ti_4O_7, but also indicates a strong interaction of the Li_2S_x with the C—Ti_4O_7 support, resulting in a significantly different chemical structure of S. In principle, a detailed fit analysis of the S 2p spectra could reveal whether the sulfur is present in an oxidation state of -2 (Li_2S), -1 (terminal sulfur [S_T] atom in Li_2S_x), or 0 (bridging sulfur [S_B] atom in Li_2S_x) for which one would expect an increase in binding energy from approximately 160 eV (Li_2S) to 161.7 eV (S_T) to 163 eV (S_B),[15] respectively. However, these binding energies seem to be significantly lower than the S $2p_{3/2}$ values we derived from the spectra of the Li_2S_x and C—Ti_4O_7/Li_2S_x. We attribute this to sample charging due to insufficient electrical contact realized by the carbon tape used for mounting the powder samples, preventing us from performing a full (quantitative) fit analysis of the recorded spectra; rather describing the spectra qualitatively. The adsorption of Li on the C—Ti_4O_7 support is corroborated by the XPS spectra of the Ti 3 s/Li 1s region (shown in Figure S9). Despite the low photoionization cross section for Li 1s electrons, a clear peak at 56.9 eV is observed for the Li_2S_x sample. The interfering presence of Ti 3 s and Ti 3p related features (see caption of Figure S9 for more details) complicate the peak assignment for the C—Ti_4O_7/Li_2S_x and C—Ti_4O_7 sample spectra. However, the corresponding difference spectrum (spectrum (d) in Figure S9) clearly visualizes the Li 1s contribution to the spectrum of the C—Ti_4O_7/Li_2S_x sample, proving the adsorption of lithium. The shift to lower binding energy compared to the Li 1s spectrum of the Li_2S_x sample and the seemingly broader spectral appearance might (similar to the finding for S, see above) indicate a support induced modification of the chemical environment of Li.
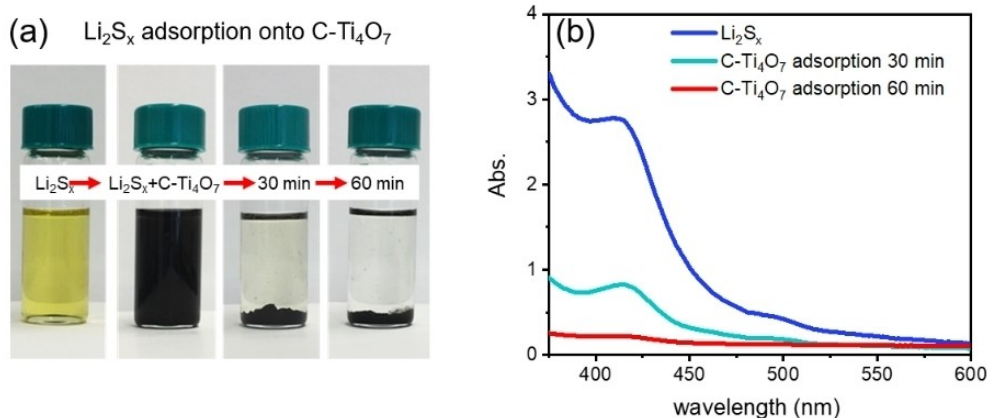

Figure 2. a) Photos of sealed vials of a Li_2S_x/DOL+DME solution: a 3 mM Li_2S_x in DOL+DME (v:v=1:1) solution, the Li_2S_x+C—Ti_4O_7 mixture upon stirring, and after standing for 30 min and 60 min, respectively. b) UV-vis absorption spectra of 3 mM Li_2S_x before and after adsorbing to C—Ti_4O_7 for 30 min and 60 min, respectively.

Batteries & Supercaps

Research Article
doi.org/10.1002/batt.202100398

Chemistry
Europe

European Chemical
Societies Publishing

Electrochemical performance of sulfur/Ti$_4$O$_7$ composites in coin cells

To evaluate the electrochemical performance of these composite electrodes for Li–S batteries, CR2032 coin cells have been first assembled with a Li-metal anode in an Ar glovebox. The electrolyte is 1 M LiTFSI in DOL/DME (1:1 by volume) with 0.5 M LiNO$_3$. The cathode consists of 60 wt% of sulfur, corresponding to an areal sulfur loading of 2 mg cm^{-2}. Cyclic voltammetry (CV) curve of the Li–S cells with C–Ti$_4$O$_7$/S as the cathode materials is shown in Figure 3(a). Two typical reduction peaks at 2.34 and 2.02 V can be observed in cycle 1, corresponding to the formation of long-chain polysulfides (Li$_2$S$_x$, $4 \leq x \leq 8$) and short-chain polysulfides (Li$_2$S$_x$, $1 \leq x \leq 4$), respectively. In the anodic scan, the oxidation peak at about 2.38 V is associated with the reverse reactions in the charging stage. Figure 3(b) shows the galvanostatic charge/discharge profiles of the C–Ti$_4$O$_7$ based cathodes. A small voltage gap
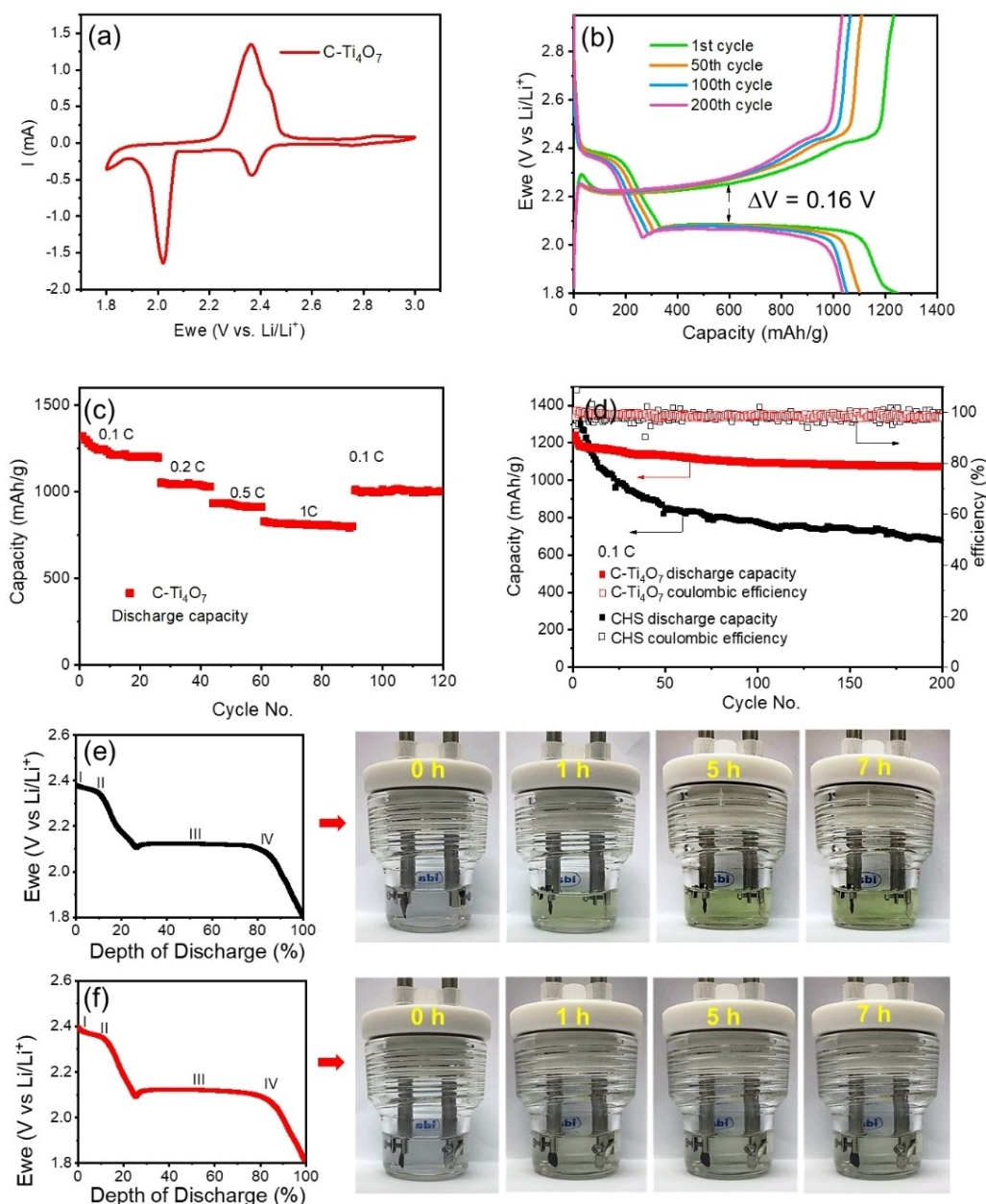

Figure 3. a) CV curve of the Li–S coin cell. b) Charge/discharge profiles of the C–Ti$_4$O$_7$/S cathode at different cycles at 0.1 C. c) Rate capabilities of the C–Ti$_4$O$_7$/S cathode at different current rates (0.1 C, 0.2 C, 0.5 C, 1 C and 0.1 C). d) Cycling performance of the C–Ti$_4$O$_7$/S cathode and the CHSs-based cathode with ~50 μL of electrolyte over 200 cycles at a charge/discharge rate of 0.1 C. The solid squares represent capacity and hollow squares represent Coulombic efficiency. e) The depth of discharge for the CHS/S cathode and its visualized beaker cell test at different times. f) The depth of discharge for the C–Ti$_4$O$_7$/S cathode and its visualized beaker cell test at different times.

Batteries & Supercaps

Research Article
doi.org/10.1002/batt.202100398

Chemistry Europe
European Chemical
Societies Publishing

($\triangle V$) of 0.16 V is found between the charge/discharge plateaus, indicating a small polarization of the battery. It is also worth noting that the ~2.1 V plateau keeps almost constant with the increasing of cycle number over 200 cycles. The stability of the plateau is related to the well-sustained fast redox kinetics of the polysulfide conversion. In our study, the C—Ti_4O_7 NPs contain highly conducting surface, which can enhance the redox electron transfer.[6d] Electrochemical impedance spectroscopy of the battery before and after cycling has been performed as shown in Figure S10. The values of total impedance of the coin cell after 5, 10, 30 times of cycling decreased gradually from ~40 Ω to ~13 Ω, indicating improved infiltration of electrolyte during the initial 30 cycles. This can be attributed to the well-defined hollow and porous structure and the polar surface of the C—Ti_4O_7 host, which enables fast ion diffusion and better interfacial property, leading to fast charge transport and facilitate the redox kinetics of sulfur conversion reaction. In addition, its porous structure provides additional physical confinement to the polysulfides, which is helpful to minimize the precipitation of lithium sulfide. In contrast, CV curve of a reference cathode made by pure carbon nanospheres with the same hollow structure (CHS, Figures S11 and S12a) shows broader redox peaks when compared to that of the C—Ti_4O_7, indicating unfavored conversion reaction of sulfur species, which may be due to the limited conductivity of the reference electrode. The voltage gap ($\triangle V$) in the charge/discharge profiles (Figure S12b) is ~0.38 V, implying a larger polarization than the C—Ti_4O_7-based battery, which is consistent with the CV curves.

The rate capabilities of the electrodes are assessed at different discharge rates from 0.1 to 1 C rate, as shown in Figure 3(c). The discharge capacity of the C—Ti_4O_7/S cathode presents a stable capacity of 1229 mAh g^{-1} at 0.1 C, 937 mAh g^{-1} at 0.2 C, 840 mAh g^{-1} at 0.5 C, and 640 mAh g^{-1} at 1 C rate, respectively. When the current density is switched to 0.1 C again, the electrode shows a reversible capacity of 998 mAh g^{-1}. The CHS/S cathode delivers a high initial capacity of 1460 mAh g^{-1} at 0.1 C, 873 mAh g^{-1} at 0.2 C, 621 mAh g^{-1} at 0.5 C, and 409 mAh g^{-1} at 1 C rate, respectively (Figure S12c). However, the discharge capacity at 0.1 C and 0.2 C shows a fast fading. When returned to 0.1 C, the discharge capacity only reaches 840 mAh g^{-1}. Figure 3(d) shows the cycling performances of the C—Ti_4O_7/S cathode at a current rate of 0.1 C, a capacity of 1050 mAh g^{-1} is obtained after 200 cycles, corresponding to 84% of the capacity retention with an average Coulombic efficiency of 98.8%. In comparison, the CHS-based cathode (Figure 3d) shows a fast fading of the initial capacity during the cycling, only 680 mAh g^{-1} of the capacity is kept after 200 cycles, corresponding to a low retention of 50%. Apparently, the C—Ti_4O_7-based cathode exhibits not only good capacity but also excellent stability due to the strong chemical binding of polysulfides to the polar surface. This efficient suppression of the shuttle effect is also revealed by a visualizable beaker cell test. Figure 3(e and f) record the color changes of beaker cells at different times (0 h, 1 h, 5 h, 7 h) during discharging. CHS/S and C—Ti_4O_7/S cathodes with the same sulfur loading are sealed in beakers, and the lithium foils

as anodes are also encapsulated. Beaker cells were discharged at 0.1 C after injecting a certain amount of electrolyte. The electrolyte color quickly turns from colorless into bright yellow in the beaker based on CHS/S cathode (Figure 3e), manifesting the dissolution and seepage of abundant lithium polysulfides into the electrolyte. For the C—Ti_4O_7/S cathode, the electrolyte color changes into slight yellow after 1 h and gets no obvious change during the discharge process, indicating very little part of lithium polysulfides are dissolved in the electrolyte (Figure 3f). This finding further substantiates the excellent confinement of polysulfides in the cathode.

XRD measurements for the C—Ti_4O_7-based cathodes before and after charging/discharging process have been conducted to study the chemical stability of Ti_4O_7. As shown in Figure S13, additional sulfur peaks can be observed in the C—Ti_4O_7/S cathode before cycling when compared to the slurry before sulfur impregnation. The characteristic peaks of Ti_4O_7 can be identified as well, demonstrating its structural stability during the sulfur impregnation process. After 10 cycles of charging/discharging at 0.2 C, the cathode was collected by disassembly of the coin cell and rinsed firstly with mixed solvent [DOL : DME = 1:1 (V:V)] and then with CS_2 to remove the lithium salts and sulfur species. The cleaned electrode clearly shows the characteristic peaks of Ti_4O_7, indicating the charging/discharging process did not destroy the crystalline structure. No obvious peaks of sulfur species have been found due to the cleaning process. Thus, both the sulfur impregnation and charging/discharging processes show no influence on the chemical structure of the C—Ti_4O_7 particles.

Electrochemical performance of sulfur/Ti_4O_7 composites in multi-layer pouch cells

One of the major advantages of the SPB templated synthesis of the C—Ti_4O_7 particles is its scalability that using a minipilot reactor results in the production of sufficient amount of materials for the construction of multilayer pouch cells. In this work, 10 g of the cathode material is produced for the fabrication of multilayer pouch cells with the cathode size of 46 mm (W) × 71 mm (L) and 500 mg sulfur loading (2 mg cm^{-2}, Figure 4a). Four pouch cells (B1–B4) have been constructed and cycled under the same cycling conditions to validate the reproducibility and reliability of the experimental results. As shown in Figure 4(a), all the four multilayer pouch cells deliver a high discharge capacity of around 1000 mAh g^{-1} at 0.05 C, demonstrating excellent reliability and high performance of the batteries. An initial discharge capacity of 830 mAh g^{-1} at 0.1 C is achieved and retained at 695 mAh g^{-1} even after 100 charge/discharge cycles (Figure 4b and c), corresponding to a capacity retention of 83.7% with a high Coulombic efficiency (CE) of 97.5%. Notably, the discharge capacity retention at the 50th cycle is even 92.3% (Figure 4c), which is much higher than many reported works of cathode development.[3e] Apart from excellent cycling stability, the C—Ti_4O_7/S cathode also delivers good rate capability. The discharge capacity of the multilayer pouch cell is stabilized at 820 mAh g^{-1} at 0.1 C, 780 mAh g^{-1} at

Batteries & Supercaps

Research Article
doi.org/10.1002/batt.202100398

**Chemistry
Europe**
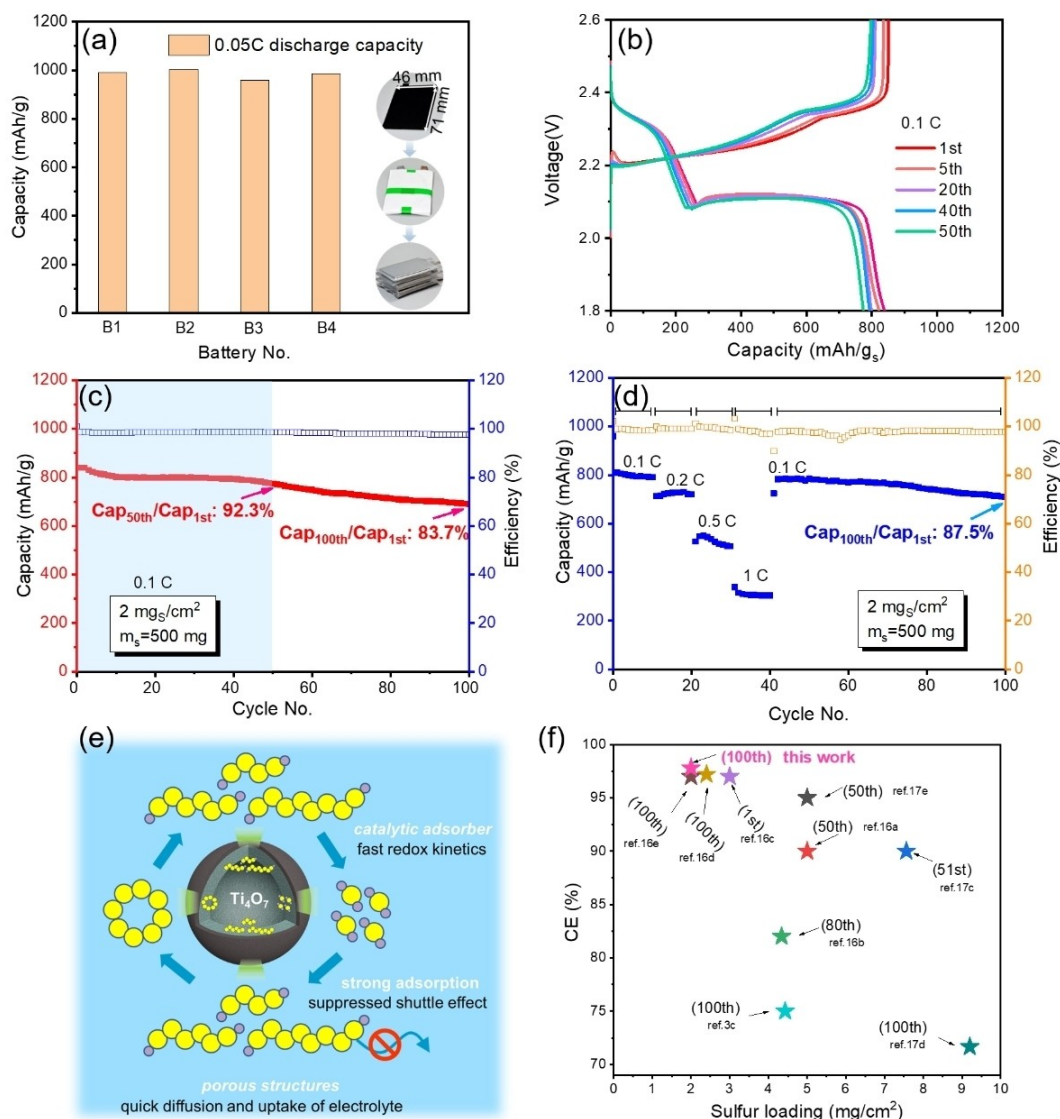European Chemical
Societies Publishing

Figure 4. Multilayer pouch cell construction and electrochemical performances. a) Charge-discharge profile of the pouch cells at 0.05 C. inset: C–Ti$_4$O$_7$/S cathode and the assembly of pouch cells. b) Charge-discharge profiles of the pouch cell at 0.1 C for different cycles. c) Cycling performance of the pouch cell for 100 cycles at a charge/discharge rate of 0.1 C. (d) Rate capabilities of the pouch cell (0.1 C, 0.2 C, 0.5 C, 1 C and 0.1 C). e) Schematic illustration of the material merits that lead to good battery performance. f) Summary of the Coulombic efficiency (CE) of different pouch cells in recent literature reports. The number in the brackets indicates the corresponding cycle No. at which the CE value was recorded. The areal sulfur loading in this work presents the loading on one side of the cathode.

0.2 C, 550 mAh g^{-1} at 0.5 C, and 320 mAh g^{-1} at 1 C rate (Figure 4d). It is worth noting that when the current density is reset to 0.1 C, the electrode shows a reversible capacity of 705 mAh g^{-1}, corresponding to a high-capacity retention of 87.5% at the 100th cycle. This excellent performance can be attributed to the synergistic advantages of the synthesized sulfur host materials (Figure 4e). A large number of 0.9–4.9 nm micro- and mesopores in the C–Ti$_4$O$_7$ particles can confine and adsorb the polysulfides by both physical and chemical interactions. Compared to typical porous carbon supports, which do not adsorb hydrophilic polysulfide intermediates, the strong surface interactions play a more crucial role in inhibiting polysulfide dissolution and deposition than confinement that relies on physical barriers. Moreover, the commonly used

polysulfide adsorbers (e.g., metal oxides, MOF, polymers) are semiconductors or even insulators with poor electrical conductivity. An additional diffusion step of polysulfides to the charge-accessible interface has to be involved to accomplish the electrochemical conversion, which profoundly reduces the electrode kinetics. Distinct to these less-conductive adsorbers, Ti$_4$O$_7$ has a high electronic conductivity.[8c] This allows the polysulfide adsorption and redox conversion to proceed on the same Ti$_4$O$_7$ site without additional diffusion to the carbon surface. Therefore, the conversion reaction can be greatly accelerated on the Ti$_4$O$_7$ surface. Thus, the prepared porous Magnéli phase C–Ti$_4$O$_7$ offers the near-optimal physical, chemical, and electronic properties to serve as an effective sulfur host. Furthermore, the thin carbon layer on the Ti$_4$O$_7$ induces

continuous conductive framework among the small Ti$_4$O$_7$ particles and the carbon black of the slurry, which enables a lower resistance and improves the electrochemical performance of the pouch cells.

Figure 4(f) summarizes the CE of selective pouch cells in recent reports, which is often disregarded due to the poor CE and short cycle life resulting from severely decreased conductivity of those high areal sulfur-loading cathodes.[16] Despite the inferior performance of cells with high areal sulfur loading, the C—Ti$_4$O$_7$/S cathode delivers an improved CE compared to those pouch cells with a comparable areal sulfur loading. More results from representative reports on Li—S pouch-cells that focused on sulfur cathode development are summarized in Figure S9.[3e,17] The pouch cell in this work outperforms others in terms of cycle life, capacity retention and specific discharge capacity. Note that the discrepancy in the sulfur loading, lithium and electrolyte amount should be fully considered for such comparison due to the strong dependence of electrochemical performances on these parameters. Although in some reports high specific energies were achieved, they were obtained with low-capacity pouch cells (usually consisting of single layer cathode) and their cycle life is often limited to only 15–50 cycles. Therefore, the multilayer Li—S pouch cell based on the porous C—Ti$_4$O$_7$ host as strong adsorber and catalytic phase represents a significant advance. With optimized cell design (e.g., optimization of the Ti$_4$O$_7$ content and location, thinner lithium foil, and perforation of Al current collector), a significantly enhanced specific energy of our Li—S pouch cell (132 Wh kg^{-1}) can be envisioned. Both rational Li metal protection technologies and cell configuration optimization (e.g., internal pressure, tortuosity/flexibility, porosity and E/S ratio) are necessary for further improvement of the cell performance.[3c,15,16c–e] In addition, scalable synthesis with more concentrated SPB beyond the present work will be a further study by applying our minipilot reactor to meet the demand of practical battery application.

Conclusion

In this work, we demonstrate a large-scale synthesis of carbon-coated hollow Ti$_4$O$_7$ nanoparticles with hierarchical porosity and high specific surface area. TiO$_2$-SPB particles are first obtained through the hydrolysis of TEOT adsorbed on the SPB templates. Hollow C—Ti$_4$O$_7$ particles are generated by the thermal reduction of the TiO$_2$-SPB particles under argon atmosphere. A thin layer of PDA is pre-coated on the surface to improve the electrical conductivity, to avoid the growth of large Ti$_4$O$_7$ crystals, and to sustain the hollow structure during the calcination. When the hollow C—Ti$_4$O$_7$ nanoparticles are used as sulfur-host materials in multilayer Li—S pouch cells, the batteries deliver a high initial discharge capacity of 1003 mAh g^{-1} at 0.05 C and an extremely stable cycling over 100 cycles with the discharge capacity retention of over 83.7 %, which is outstanding compared to previous reports. In short, this work realizes the large-scale synthesis of C—Ti$_4$O$_7$ particles with well-controlled porous structures, which has been demon-

strated to be highly efficient sulfur host materials for multilayer pouch cells, paving the way for the transfer of nanostructured functional materials from lab cell to the prototype cell level. This facile synthesis is possible to be extended to a wide range of functional particles such as other metal oxides/sulfides particles, providing a practical technique for the production of efficient cathode materials with superiority in advanced nanostructure and large-scale synthesis.

Experimental Section

Synthesis of the TiO$_2$-SPB composite particles

The SPB templates were synthesized according to previous report.[18] A two-step procedure including the synthesis of photo-initiator-decorated PS cores and the grafting of polyelectrolyte brushes was conducted. Firstly, the PS core particles covered with a thin layer of photoinitiator, 2-[p-(2-Hydroxy-2-methylpropiophenone)]-ethyleneglycol methacrylate (HMEM), were prepared by conventional emulsion polymerization, which has been described in detail previously.[19] Secondly, the polyelectrolyte brushes were prepared by photo-emulsion polymerization. Functional monomer styrene sulfonic acid sodium salt (NaSS; Aldrich, 30 mol % with regard to the amount of styrene) was mixed with diluted PS core solution (2.5 wt %) under stirring. Photo-emulsion polymerization was conducted under UV irradiation at room temperature for 60 min. The brush particles were cleaned by ultrafiltration firstly against DI water (membrane: cellulose nitrate with 100 nm pore size) and followed by ethanol (membrane: regenerated cellulose with 100 nm pore size).

For the synthesis of TiO$_2$ nanocomposite particles, 10 g PS-NaSS brush particles were dispersed in 3 L ethanol in a minipilot reactor. Water with a stoichiometric ratio of TEOT ($V_{H2O}:V_{TEOT} = 1:10$) was then added while stirring. The reaction was initiated by adding the solution of 15 mL tetraethylorthotitanate (TEOT) dissolved in 500 mL ethanol. The TEOT solution was added drop wise at a feeding rate of 10 mL min^{-1}. The reaction mixture was stirred vigorously for two more hours after the complete addition of TEOT solution at room temperature. The TiO$_2$-SPB particles were then washed with ethanol and water by repeated centrifugation 3 times and redispersed into Tris buffer solution after cleaning.

Synthesis of the carbon-coated Ti$_4$O$_7$ hollow particles (C—Ti$_4$O$_7$ NPs)

The TiO$_2$-SPB particles obtained from 10 g SPB templates were centrifuged and redispersed into a solution of dopamine hydrochloride (0.5 g L^{-1}) dissolved in Tris buffer (3 L, pH 8.5–8.8). The reaction solution was kept around 0 °C for 2 h then at room temperature for more than 7 h with vigorous stirring. After the PDA deposition, the samples were collected by centrifugation at 6000 rpm for 10 min. The secondary PDA particles were removed by repeated centrifugation until the supernatant was colorless. The PDA@TiO$_2$-SPB particles were collected by freeze drying and heated at 100 °C for 4–6 h, then calcined at 950 °C for 4 h to remove the PS cores and release the hollow structure. At the same time, the TiO$_2$ was partially reduced into Ti$_4$O$_7$ phase using the carbon residuals from the polymer template as reducing agent. The calcination was conducted under an Ar stream in a tubular furnace using a heating ramp of 4 °C min^{-1}. The reference materials, pure carbon hollow nanospheres (CHS) were synthesized following the same procedure but without usage of TEOT.

Materials characterizations

The hollow structure of the obtained particles was investigated by the transmission electron microscopy (TEM) using JEOL JEM-2100 (JEOL GmbH, Eching, Germany) at an acceleration voltage of 200 kV. The scanning electron microscopy (SEM) imaging and energy-dispersive X-ray spectroscopy (EDX) elemental mapping were performed using a LEO 1530 field emission SEM equipped with an EDX attachment (Zeiss) measurement in secondary electron mode at 2 kV. X-ray diffraction (XRD) measurements were performed in a Bruker D8 diffractometer in the locked coupled mode (2θ ranging from 10° to 80°) with Cu Kα1 radiation. N_2 adsorption/desorption isotherms were obtained using a Quantachrome Autosorb-1 system at 77 K. The samples were degassed at 250 °C for 12 h before measurement. Specific surface areas were calculated using the Brunauer-Emmett-Teller method based on a multipoint analysis. The X-ray photoelectron spectroscopy (XPS) measurements were performed in the EMIL laboratory using a non-monochromatized PREVAC RS40B1 Mg K_α/Al K_α twin anode X-ray source and a ScientaOmicron Argus CU electron analyzer in ultra-high vacuum (UHV, base pressure $< 1 \times 10^{-9}$ mbar) conditions. Energy calibration has been realized by measuring a clean gold foil sample and adjusting the peak position of the Au $4f_{5/2}$ peak to 84.00 eV. The studied samples have been loaded into the UHV system via an Ar-filled glovebag to minimize air exposure.

Adsorption of lithium polysulfides to the host materials

Firstly, visualized adsorption tests were conducted by mixing desired amount of lithium polysulfide solution with C–Ti_4O_7 NPs for some time and comparing the change of solution color before and after placing for 1 h. The lithium polysulfide solution was prepared with sulfur (67.2 mg) and lithium sulfide powder (13.8 mg) in a molar ratio of 7:1 into 100 mL DME+DOL (v/v, 1:1). The mixture was aged at 80 °C for 48 h in the glovebox to obtain the brown mixture of Li_2S_x solution. 20 mg of host material powders was added into 2 mL of Li_2S_x solution (theoretically equivalent to 3 mM Li_2S_8 solution), respectively. After aging 1 h in the glovebox, the supernatant liquid was sealed in cylinder quartz for UV-vis spectroscopy test. The Li_2S_x treated C–Ti_4O_7 sample was firstly collected via centrifugation and then cleaned with THF and toluene for one time, respectively, to remove the access amount of sulfur species before XPS measurement.

Battery assembly and electrochemical measurements

The sublimed sulfur powder was mixed with C–Ti_4O_7 in the mass ratio of 6:4 and heated at 155 °C for 12 h to incorporate sulfur into the host materials. The coin cells were assembled in an Ar-filled glovebox with the concentration of moisture and oxygen below 1.0 ppm. CR 2032 coin cells were fabricated by assembling a single-sided C–Ti_4O_7/S cathode ($D=14$ mm), a 25 μm Celgard 2500 separator, and a 250 μm lithium foil anode ($D=16$ mm). The electrolyte (E/S = 17 μL mg^{-1}) contains 1 M Li bis(trifluoromethane)sulfonamide (LiTFSI) and 0.5 M lithium nitride (LiNO$_3$) in a mixture solution of 1,3-dioxolane (DOL) and 1,2-dimethoxyethane (DME) (1:1 by volume). The galvanostatic charge/discharge tests were performed using a Biologic electrochemical workstation (MPG2 galvanostat/potentiostat) at different current densities within a cut-off voltage window of 1.8–3.0 V. The specific capacity is calculated based on the mass of S with a theoretical capacitance of 1675 mAh g^{-1}.

A transparent beaker cell was built to verify the polysulfide formation and shuttle using a 10 mL glass vial. The cell contains 5 mL of the electrolyte with the same composition, which is much more than a regular coin cell. A piece of lithium foil and C–Ti_4O_7/S cathode were immersed in the electrolyte. The cell was discharge at 0.05 C to provide a visible change of the sulfur species in the cathode. The formation and movement of polysulfides can be directly visualized and recorded at different times.

To assemble the 500 mg sulfur loading pouch cell, we added 833 mg C–Ti_4O_7/S powder, 104 mg carbon black, 104 mg polyvinylidene fluoride (PVDF) binder to a suitable amount of N-methyl-2-pyrrolidone (NMP). The resulting slurry was casted on the both sides of Al foil. After drying at room temperature for 16 h, the cathode was transferred into a 60 °C vacuum oven overnight. The typical areal loading of S was 2.0 mg cm^{-2}. The double-sided cathode was cut into 46 mm by 71 mm. The Al tab was riveted on the as-prepared cathode, and a Ni tab was riveted on the Li foil (46 mm by 71 mm) with a thickness of 100 μm. Then, we stacked Celgard 2500 on the surface of the Li foil, followed by the cathode on the top of the Celgard 2500 separator. The process was repeated until three double-sided cathodes and two single-sided cathodes were assembled. The electrolyte was used the same with that of the coin cell, containing 1 M Li bis(trifluoromethane)sulfonamide (LiTFSI) and 0.5 M lithium nitride (LiNO$_3$) in a mixture solution of 1,3-dioxolane and 1,2-dimethoxyethane (1:1 by volume). 2.5 mL electrolyte (E/S = 5 μL mg^{-1}) was injected into the stack. Finally, the package was sealed under vacuum. The galvanostatic charge/discharge tests were performed at 0.05 C for 1 cycle followed with cycling at 0.1 C for over 100 cycles. Different C-rates (0.1 C, 0.2 C, 0.5 C and 1 C) were also investigated within a cutoff voltage window of 1.8–2.6 V. The specific energy density was calculated based on the total weight of the whole pouch cell (including the electrode materials, additives, current collectors, electrolytes and the pouch itself).

Acknowledgements

Conflict of Interest

The authors declare no conflict of interest.

Data Availability Statement

The data that support the findings of this study are available from the corresponding author upon reasonable request.

[1] a) M. Wild, L. O'Neill, T. Zhang, R. Purkayastha, G. Minton, M. Marinescu, G. J. Offer, *Energy Environ. Sci.* **2015**, *8*, 3477–3494; b) M. Armand, J. M. Tarascon, *Nature* **2008**, *451*, 652–657; c) A. Manthiram, Y. Fu, S.-H. Chung, C. Zu, Y.-S. Su, *Chem. Rev.* **2014**, *114*, 11751–11787; d) T. Li, X.

Batteries & Supercaps

Research Article
doi.org/10.1002/batt.202100398

Chemistry Europe
European Chemical
Societies Publishing

Bai, U. Gulzar, Y.-J. Bai, C. Capiglia, W. Deng, X. Zhou, Z. Liu, Z. Feng, R. Proietti Zaccaria, *Adv. Funct. Mater.* **2019**, *29*, 1901730; e) X. Zhang, Y. Wei, B. Wang, M. Wang, Y. Zhang, Q. Wang, H. Wu, *Nano-Micro Lett.* **2019**, *11*, 78.

[2] a) S. Evers, L. F. Nazar, *Acc. Chem. Res.* **2013**, *46*, 1135–1143; b) X. Ji, K. T. Lee, L. F. Nazar, *Nat. Mater.* **2009**, *8*, 500–506; c) W. Ren, W. Ma, S. Zhang, B. Tang, *Energy Storage Mater.* **2019**, *23*, 707–732; d) J. Zhang, Z. Li, Y. Chen, S. Gao, X. W. Lou, *Angew. Chem. Int. Ed.* **2018**, *57*, 10944–10948; *Angew. Chem.* **2018**, *130*, 11110–11114; e) X. Liu, J. Q. Huang, Q. Zhang, L. Mai, *Adv. Mater.* **2017**, *29*, 1601759.

[3] a) S. Dörfler, H. Althues, P. Härtel, T. Abendroth, B. Schumm, S. Kaskel, *Joule* **2020**, *4*, 539–554; b) J. He, Y. Chen, A. Manthiram, *Energy Environ. Sci.* **2018**, *11*, 2560–2568; c) X.-B. Cheng, C. Yan, J.-Q. Huang, P. Li, L. Zhu, L. Zhao, Y. Zhang, W. Zhu, S.-T. Yang, Q. Zhang, *Energy Storage Mater.* **2017**, *6*, 18–25; d) M. Shaibani, M. S. Mirshekarloo, R. Singh, C. D. Easton, M. C. D. Cooray, N. Eshraghi, T. Abendroth, S. Dörfler, H. Althues, S. Kaskel, A. F. Hollenkamp, M. R. Hill, M. Majumder, *Sci. Adv.* **2020**, *6*, eaay2757; e) C. Zhao, G.-L. Xu, Z. Yu, L. Zhang, I. Hwang, Y.-X. Mo, Y. Ren, L. Cheng, C.-J. Sun, Y. Ren, X. Zuo, J.-T. Li, S.-G. Sun, K. Amine, T. Zhao, *Nat. Nanotechnol.* **2021**, *16*, 166–173.

[4] K. Zhu, C. Wang, Z. Chi, F. Ke, Y. Yang, A. Wang, W. Wang, L. Miao, *Front. Energy Res.* **2019**, *7*, 123.

[5] a) A. Eftekhari, D.-W. Kim, *J. Mater. Chem. A* **2017**, *5*, 17734–17776; b) L. Yang, Q. Li, Y. Wang, Y. Chen, X. Guo, Z. Wu, G. Chen, B. Zhong, W. Xiang, Y. Zhong, *Ionics* **2020**, *26*, 5299–5318.

[6] a) S. Yao, R. Guo, Z. Wu, M. Liu, X. Qian, X. Shen, T. Li, L. Wang, Y. Wang, S. Qin, *J. Electroceram.* **2020**, *44*, 154–162; b) M. Liu, S. Jhulki, Z. Sun, A. Magasinski, C. Hendrix, G. Yushin, *Nano Energy* **2021**, *79*, 105428; c) Y. Guo, J. Li, R. Pitcheri, J. Zhu, P. Wen, Y. Qiu, *Chem. Eng. J.* **2019**, *355*, 390–398; d) Q. Pang, D. Kundu, M. Cuisinier, L. F. Nazar, *Nat. Commun.* **2014**, *5*, 4759; e) X. Wu, S. Yao, M. Liu, S. Pang, X. Shen, T. Li, S. Qin, *Ionics* **2021**, *27*, 2397–2408; f) F. Wang, X. Ding, R. Shi, M. Li, Y. Lei, Z. Lei, G. Jiang, F. Xu, H. Wang, L. Jia, R. Jiang, Z. Liu, J. Sun, *J. Mater. Chem. A* **2019**, *7*, 10494–10504; g) Z. Li, J. Zhang, B. Guan, D. Wang, L.-M. Liu, X. W. Lou, *Nat. Commun.* **2016**, *7*, 13065; h) H. Wakayama, K. Yamazaki, *ACS Omega* **2021**, *6*, 4161–4166.

[7] a) J. R. Smith, F. C. Walsh, R. L. Clarke, *J. Appl. Electrochem.* **1998**, *28*, 1021–1033; b) L. Liborio, G. Mallia, N. Harrison, *Phys. Rev. B* **2009**, *79*, 245133.

[8] a) F. C. Walsh, R. G. A. Wills, *Electrochim. Acta* **2010**, *55*, 6342–6351; b) X. Zhong, I. Rungger, P. Zapol, O. Heinonen, *Phys. Rev. B* **2015**, *91*, 115143; c) S. Harada, K. Tanaka, H. Inui, *J. Appl. Phys.* **2010**, *108*, 083703.

[9] S. Risse, E. Härk, B. Kent, M. Ballauff, *ACS Nano* **2019**, *13*, 10233–10241.

[10] a) J. Ye, G. Wang, X. Li, Y. Liu, R. Zhu, *J. Mater. Sci. Mater. Electron.* **2015**, *26*, 4683–4690; b) R. Zhu, Y. Liu, J. Ye, X. Zhang, *J. Mater. Sci. Mater. Electron.* **2013**, *24*, 4853–4856; c) C. Tang, D. Zhou, S. Fang, L. Yang, *J. Electrochem. Soc.* **2012**, *159*, A1796–A1800.

[11] H. Wei, E. F. Rodriguez, A. S. Best, A. F. Hollenkamp, D. Chen, R. A. Caruso, *Adv. Energy Mater.* **2017**, *7*, 1601616.

[12] S. Mei, C. J. Jafta, I. Lauermann, Q. Ran, M. Kärgell, M. Ballauff, Y. Lu, *Adv. Funct. Mater.* **2017**, *27*, 1701176.

[13] M. Schrinner, B. Haupt, A. Wittemann, *Chem. Eng. J.* **2008**, *144*, 138–145.

[14] X. Tao, J. Wang, Z. Ying, Q. Cai, G. Zheng, Y. Gan, H. Huang, Y. Xia, C. Liang, W. Zhang, Y. Cui, *Nano Lett.* **2014**, *14*, 5288–5294.

[15] a) X. Liang, C. Hart, Q. Pang, A. Garsuch, T. Weiss, L. F. Nazar, *Nat. Commun.* **2015**, *6*, 5682; b) V. Shutthanandan, M. Nandasiri, J. Zheng, M. H. Engelhard, W. Xu, S. Thevuthasan, V. Murugesan, *J. Electron Spectrosc. Relat. Phenom.* **2019**, *231*, 2–10.

[16] a) L. Luo, S.-H. Chung, H. Yaghoobnejad Asl, A. Manthiram, *Adv. Mater.* **2018**, *30*, 1804149; b) M.-S. Kim, M. S. Kim, V. Do, Y. Xia, W. Kim, W. I. Cho, *J. Power Sources* **2019**, *422*, 104–112; c) J. Zhang, C.-P. Yang, Y.-X. Yin, L.-J. Wan, Y.-G. Guo, *Adv. Mater.* **2016**, *28*, 9539–9544; d) C. Kensy, P. Härtel, J. Maschita, S. Dörfler, B. Schumm, T. Abendroth, H. Althues, B. V. Lotsch, S. Kaskel, *Carbon* **2020**, *161*, 190–197; e) J. Kulisch, H. Sommer, T. Brezesinski, J. Janek, *Phys. Chem. Chem. Phys.* **2014**, *16*, 18765–18771.

[17] a) W. Xue, Z. Shi, L. Suo, C. Wang, Z. Wang, H. Wang, K. P. So, A. Maurano, D. Yu, Y. Chen, L. Qie, Z. Zhu, G. Xu, J. Kong, J. Li, *Nat. Energy* **2019**, *4*, 374–382; b) Z. Fang, Y. Luo, H. Wu, L. Yan, F. Zhao, Q. Li, S. Fan, J. Wang, *Carbon* **2020**, *166*, 183–192; c) F. Wu, Y.-S. Ye, J.-Q. Huang, T. Zhao, J. Qian, Y.-Y. Zhao, L. Li, L. Wei, R. Luo, Y.-X. Huang, Y. Xing, R.-J. Chen, *ACS Nano* **2017**, *11*, 4694–4702; d) O. Salihoglu, R. Demir-Cakan, *J. Electrochem. Soc.* **2017**, *164*, A2948-A2955; e) L. Luo, J. Li, H. Yaghoobnejad Asl, A. Manthiram, *ACS Energy Lett.* **2020**, *5*, 1177–1185.

[18] Y. Lu, M. Hoffmann, R. S. Yelamanchili, A. Terrenoire, M. Schrinner, M. Drechsler, M. W. Möller, J. Breu, M. Ballauff, *Macromol. Chem. Phys.* **2009**, *210*, 377–386.

[19] M. Ballauff, *Prog. Polym. Sci.* **2007**, *32*, 1135–1151.